Magnetic Resonance Imaging of Chemical EOR in Core to Complement Field Pilot Studies

J. Mitchell[a], J. Staniland[b], A. Wilson[b], A. Howe[b], A. Clarke[b], E.J. Fordham[b], J. Edwards[c], R. Faber[d] and R. Bouwmeester[d]

[a] Department of Chemical Engineering and Biotechnology, University of Cambridge, New Museums Site, Pembroke Street, Cambridge, CB2 3RA, UK.
[b] Schlumberger Cambridge Research, High Cross, Madingley Road, Cambridge, CB3 0EL, UK.
[c] Schlumberger Oman & Co, LLC, PO Box 2548, Ruwi, Postal Code 112, Sultanate of Oman.
[d] Shell Global Solutions International BV, Kessler Part 1, 2288GS Rijswijk, The Netherlands.

This paper was prepared for presentation at the International Symposium of the Society of Core Analysts held in Aberdeen, Scotland, UK, 27-30 August, 2012

Abstract

Before possible multi-well pilots and full field-scale implementation, chemical enhanced oil recovery (EOR) projects usually follow an incremental screening procedure from the laboratory through single-well pilots. Laboratory-scale core floods at reservoir conditions validate surfactant performance before committing to field trials. However, in single short plugs, volumetric averages do not correctly quantify remaining oil due to capillary end effects, oil banks, and other flow heterogeneities. Magnetic resonance imaging (MRI) protocols extend traditional core floods and allow quantitative resolution of non-uniform saturation on millimetre length scales. At low magnetic field strengths, MRI data correspond directly to the measurement physics of nuclear magnetic resonance (NMR) logging tools. NMR and dielectric dispersion tools are ideal for quantifying remaining oil in single-well field trials, being independent of Archie parameters which are uncertain under complex salinity and wettability distributions. We report a laboratory study on short core plugs from a North Oman carbonate field, confirming the efficacy of an alkaline surfactant (AS) formulation at reservoir conditions. Good injectivity of surfactant was seen in selected reservoir material, suggesting that surfactant formulation was not responsible for inconsistent injectivity seen in single well field tests using a log-drill-inject-log pilot protocol. The low-field MRI results corroborate oil saturation changes seen by wireline logs on a decimetre length scale in the single-well field test. Remaining oil determinations can thus be compared at various length scales ranging from millimetres (MRI), to decimetres (log-drill-inject-log pilots), and finally to field scale trials using single well chemical tracer tests.

Introduction

Determination of the effectiveness of EOR agents begins at the laboratory scale [1]. A possible EOR agent for a given reservoir is identified and then adjusted to provide the required fluid-phase behavior. In the case of surfactants, a reduction in interfacial tension (IFT) is required. Refinements in the chemical design ensure compatibility with reservoir salinity, temperature, and crude. Laboratory-scale core floods are then conducted prior to piloting in the reservoir. A single-well *in situ* EOR evaluation has recently been introduced [2,3] involving a log-drill-inject-log sequence with injection into a sidewall hole. In the laboratory, oil recovery is monitored in an environment adjusted to match reservoir conditions, using downhole core and oil. Here, an AS formulation was chosen for compatibility with a light crude oil and low salinity brine. The field in North Oman [4,5] contains a layer of microporous limestone. Several plugs extracted from cored reservoir material were provided for the laboratory-scale investigations. The core floods were monitored using rapid NMR measurements of spatially resolved T_2 relaxation time distributions, providing direct comparability to the data acquired in a standard NMR well log, albeit on a smaller length scale [6]. Two core floods were completed in the laboratory with differing volumes of AS injection. In the first flood, a large volume of AS was injected to mimic the observations of the wireline tools being sensitive only to saturation states near the well bore. In the second flood, a smaller quantity of AS was injected to emulate the EOR process further away from the well bore.

To determine the remaining oil saturation (ROS) in an NMR measurement, it is necessary to distinguish between signal arising from the oil and brine (or other aqueous fluid-phases, such as the AS) present in the core-plug. Various methods are available for fluid-type discrimination, including relaxation time, diffusion coefficient, and chemical spectroscopy. However, at low magnetic fields chemical selectivity is not available, and given the combination of a light oil and a weakly-relaxing carbonate formation in this study, neither relaxation nor diffusion contrast alone provides unambiguous fluid-typing.

For the corresponding single-well *in situ* EOR pilot [5] injectivity problems resulted in a small flooded zone for which the vertical resolution of NMR logging was inadequate. NMR logging was carried out prior to injection, but logging after injection was abandoned. Wideband dielectric measurements, with their finer spatial resolution, then became the measurement of choice. Nevertheless, in the absence of injectivity problems, the combination of joint diffusion-relaxation NMR measurements, and wideband dielectric measurements, remains a viable combination for the single-well *in situ* EOR pilot, and the laboratory NMR response at various stages of the flood is of high value for full interpretation of the downhole data.

At the laboratory-scale, because of the challenging combination of a light oil in a weakly-relaxing carbonate formation, in this work we achieve NMR fluid-phase contrast by substituting heavy water (D_2O) in all the aqueous fluid-phases. As the NMR signal is obtained only from ^1H, heavy water is not observed. D_2O has been used previously to validate the linear response of NMR signal intensity with oil saturation [7] and also to provide fluid-phase contrast in MRI of rock cores [8,9].

In laboratory-scale core floods it is desirable to use long plugs (length ≥ 300 mm) to ensure end effects and other flow heterogeneities do not dominate the results from bulk measurements of remaining oil, such as gravimetric assay of the effluent. However, such plugs can be difficult to extract and it may be necessary to construct composite cores from shorter plugs. Existing commercial NMR systems are not suited to bulk measurements of such long samples, and some form of mechanical scanning is required to assess the entire sample, limiting the capability to monitor a core flood continuously. Here, then, we utilize MRI protocols to provide spatially resolved oil saturations within a short core plug (length 50 mm). We have previously demonstrated that quantitative oil saturations, consistent with well logs, are obtained from such short plugs when an appropriate region of the sample, being free from capillary or geometry end effects, is monitored [6]. While MRI of rock cores has an intermittent history spanning over three decades, the implementation of imaging protocols on low-field NMR systems comparable to wireline tools is a recent addition in core analysis. Previously, MRI of rocks was typically implemented on high-field medical MRI scanners that often do not provide quantitative results due to magnetic susceptibility contrast between the solid and liquid, which is known to scale with field strength [10]. The magnetic susceptibility contrast also limits the maximum resolution in MRI of rocks to around $\Delta y \sim 100$ μm [11]; therefore, it is not possible to resolve individual pores at any field strength. Implementation of MRI on a magnet with a field strength of $B_0 = 50$ mT is accompanied by a reduction in the imaging resolution achievable in a reasonable time due to the inherent poor signal-to-noise ratio (SNR), compared to that obtainable at a field strength of, say, $B_0 = 2$ T. Nevertheless, low-field MRI is still invaluable in core analysis as the flow heterogeneities of interest occur on millimeter to centimeter length scales and are thus observable despite the low resolution.

Experimental Procedures

The NMR metric of choice in well logging is the T_2 relaxation time, being readily measured downhole. In the laboratory, we measure T_2 using the standard Carr-Purcell Meiboom-Gill (CPMG) [12,13] pulse sequence. In natural porous media, it is assumed that a continuous distribution of pore sizes exist [14], so a continuous distribution of relaxation time components, $f(T_2)$, will be observed; the integral of $f(T_2)$ is proportional to saturation. Accordingly, the magnetization g of the n^{th} echo observed at time nt_E will be described by the first kind Fredholm integral equation

$$\frac{g(nt_E)}{g(0)} = \int_0^\infty \exp\left\{-\frac{nt_E}{T_2}\right\} f(T_2)\,\mathrm{d}(\log_{10} T_2) + \varepsilon\,, \tag{1}$$

where ε is the experimental noise. We solve this ill-posed problem for T_2 on the $\log_{10}$ scale using Tikhonov regularization [15] with a smoothing parameter determined by the generalized cross validation (GCV) method [16].

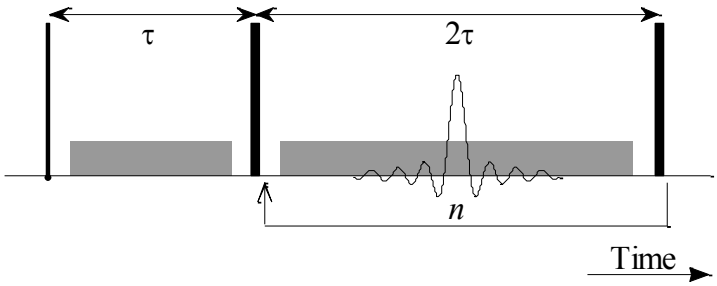

Figure 1. NMR pulse sequence used to acquire y-T_2 maps. The thin and thick vertical lines represent 90º and 180º rf pulses, respectively. The 180º refocusing pulses are separated by time $2\tau = t_E$. The grey rectangles represent magnetic field gradient pulses of amplitude G_y. The echo is acquired in the presence of the gradient to provide spatial (frequency) encoding. A total of n echoes are recorded, each containing m complex data with a dwell time of Δt.

Spatial resolution (MRI) is achieved with a frequency encoded spin echo [17]. By acquiring multiple echoes, a spatially resolved map of T_2 distribution is obtained [18]. This is known as "RARE" in medical MRI. Details of the processing stages are to appear elsewhere [6]. A schematic of the multi-echo imaging pulse sequence is shown in Fig. 1.

NMR data were acquired continuously throughout the core floods. Basic CPMG experiments were interleaved with y-T_2 maps. For the basic CPMG experiments, n = 1024 and t_E = 300 μs. For the y-T_2 maps, n = 128, t_E = 1 ms, G_y = 2.7 G cm^{-1}, m = 64, and Δt = 10 μs. The resultant field of view in the profiles was FOV = 8.6 cm with a resolution of Δy = 1.3 mm. Each CPMG acquisition had a duration of 5 min, and each y-T_2 map was acquired in 15 min. Therefore, NMR data acquisitions were completed every 20 min during the continuous flood.

All the NMR experiments were conducted on an Oxford Instruments {Abingdon, Oxon, UK} Maran DRX2-HF spectrometer using a "Big-2" magnet operating at B_0 = 56 mT with a resonant frequency of f_0 = 2.4 MHz for ^{1}H. The magnet was equipped with a 53 mm diameter solenoid resonator and single y-axis magnetic field gradient coils. The core-plugs were confined in a NMR-compatible core-holder manufactured by ErgoTech {Conwy, UK}. Temperature and confining pressure were supplied by a perfluorinated oil {Fluorinert^{TM} FC-40, 3M Chemical Products Inc}. The confining pressure was raised by dual-cylinder piston pumps {model 500 D, Teledyne-ISCO, Lincoln, NE}. The core floods were performed at the reservoir temperature of 69ºC and an isostatic confining pressure of 3 MPa. A single cylinder piston pump {model 260D, Teledyne-ISCO} was used to inject the flooding fluids at a constant volumetric rate of 0.084 cm^3 min^{-1}, corresponding to a linear velocity of 1 ft day^{-1} in the formation. For each flood, the aqueous fluid-phases were injected in the order: {brine, AS, brine} at varying volumes. Summaries of the floods are given in Table 1.

Inlet, outlet, and differential pressure were recorded throughout the flood. The effluent was collected as small aliquots in sealed vials for analysis. The fraction of anionic surfactant recovered in the aqueous fluid-phase was determined spectrophotometrically using the cationic dye methylene blue, a standard waste-water management assay [19].

Table 1. Flood protocols showing volume of each aqueous fluid-phase injected into the core-plugs.

Plug	Duration / h	Volume pumped / cm^3	Cumulative volume pumped / PV	Fluid
A	46.90	236.4	15.5	Brine
	24.25	122.2	23.5	AS
	6.21	31.30	25.5	Brine
B	40.73	205.3	13.6	Brine
	6.73	33.94	15.8	AS
	21.37	107.7	22.9	Brine

The surfactant-dye complex was extracted into an immiscible organic solvent (chloroform) and the concentration determined using high-performance liquid chromatography (HPLC) coupled with a photo-diode array (PDA).

Materials

Synthetic brine was formulated using D_2O for both the formation and injection water. A variety of sodium and potassium salts were included and the final brine preparation had a total dissolved solids content of 10 g dm^{-3}. At the reservoir temperature of 69ºC, the brine had a density of ρ_w = 1.061 g cm^{-3}. The AS was prepared by adding 0.3 wt% tridecylalcohol propoxy sulfate (Petrostep S-8A surfactant), 3 wt% diethylene glycol monobutyl ether (DGBE co-solvent), and 1.75 wt% sodium carbonate (alkali) to the D_2O brine. The AS density at 69ºC was ρ_w = 1.107 g cm^{-3}.

The dead crude oil was mixed with hexane at 35 wt% to emulate the downhole properties of live crude oil: density ρ_o = 0.7413 g cm^{-3} (API gravity 49.6º) at 69ºC; viscosity 1.87 mPa s was determined at ambient conditions (elevated temperature measurements not being possible due to the volatile content). Interfacial tension between the crude oil and AS was measured from ambient to 48ºC, where γ_{ow} = 0.01 mN m^{-1}; based on the variation of IFT with temperature, an ultra-low IFT γ_{ow} < 0.003 mN m^{-1} was predicted at the reservoir temperature.

Table 2. Physical properties of limestone plugs used in NMR monitored core flood experiments.

Plug	Well depth / m	Bulk volume / cm^3	Grain density / g cm^{-3}	Grain volume / cm^3	Pore volume / cm^3	Porosity / p.u.	Permeability / mD	$S_o^{(init)}$ / s.u.
A	xx89.3	52.30	2.703	36.90	15.27	29.3	6.8	92.3
B	xx88.7	52.41	2.703	36.96	15.15	29.1	5.6	93.2

The limestone core-plugs were well-consolidated with a uniform texture. The pore structure is dominated by microporosity. The core-plugs were cleaned following a standard Soxhlet procedure. Gas porosity and Klinkenberg permeability measurements were made on the cleaned, dried plugs. The physical properties are summarized in Table

2. The plugs were vacuum saturated with synthetic D_2O brine for 12 h before being spun under oil in a centrifuge at 7500 rpm for 36 h. The initial oil saturation was determined volumetrically as $S_o \approx 93$ s.u. High oil saturation was facilitated by the large density difference between the oil and D_2O brine. Finally, the plugs were aged 4 weeks in oil at 69ºC under 275 kPa pressure, attempting, apparently successfully, to restore downhole wettability. Bump floods were not used. Oil-wet capillary end effects were indeed observed in the NMR image profiles, confirming restoration of an oil-wetting condition.

Results

The spatial variation in oil saturation along plug **A** is shown in Figure 2 as a function of flood progress (PV of injected fluid). The recovery protocol, given in Table 1, included the injection of 8 PV AS. This flood is therefore an emulation of the recovery expected at the well bore during a local pilot (as observed by wireline logs). Approximately 62 s.u. oil is recovered during the initial brine flood and a long tail of reducing oil saturation is observed as brine injection continued. A capillary end effect (high remaining oil at end of water flood, $S_{or}^{(w)}$) is observed at the outlet face of the plug due to the change in wettability and permeability between the rock and the core-holder distribution plate. The injection of the AS causes notable changes in the oil saturation: the bulk remaining oil saturation is reduced from $S_{or}^{(w)} = 25$ s.u. (remaining oil at end of water flood) to $S_{or}^{(c)} = 16$ s.u. (remaining oil at end of chemical flood), and the capillary end effect is removed. An oil bank (increase in local S_o) is observed as the AS mobilizes and transports trapped oil through the plug. Continued injection of AS resulted in further displacement of oil at the inlet region, attributed to the transport of a microemulsion. The final, bulk oil saturation was $S_{or} = 14$ s.u.

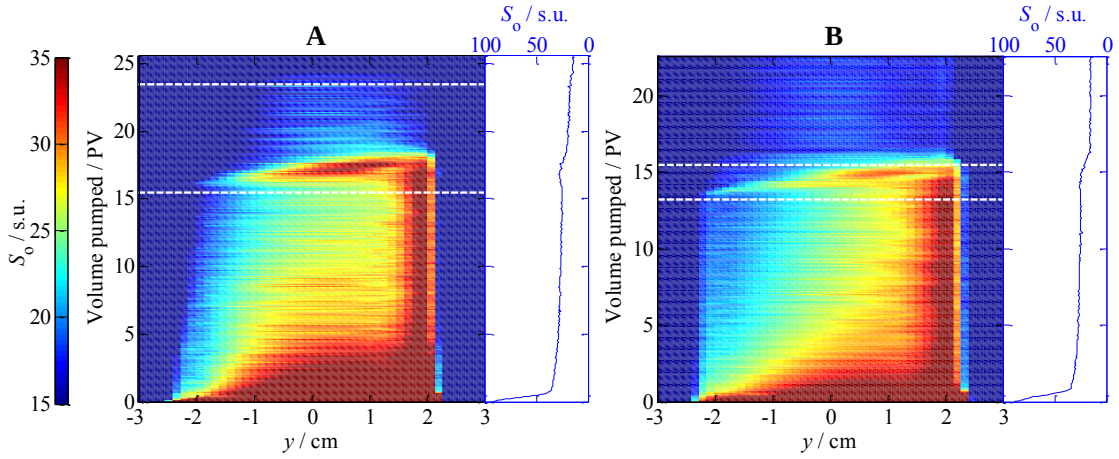

Figure 2. Spatially resolved oil saturations in plugs **A** and **B** during the brine and AS flood. The inlet face of the plug is located at y = -2.5 cm and the outlet at y = 2.5 cm. Fluid flow occurred from left to right; AS injection occurred between the horizontal dashed lines. The variation in bulk oil saturation is shown projected on the right of each plot. For both plugs, an initial piston-like displacement **o**f oil is observed followed by a gradual recovery during the brine flood; elevated oil saturation is observed at the outlet: this is a capillary end effect. On AS injection, increased mobility of the oil leads to the transport of an oil bank (increased local S_o) through the plug; the AS also removes the capillary end effect. In plug **A**, the continued injection of surfactant results in additional oil recovery at the inlet. Outlet capillary has negligible volume so S_o essentially zero for $y > 2.5$ cm.

An almost identical recovery process is observed in plug **B** with the exception that the reduced volume of injected AS (2.4 PV) did not elicit additional recovery at the inlet region of the plug. Notwithstanding, the other salient features were observed (oil bank formation, removal of capillary end effect), indicating that the AS would be effective at enhancing the oil recovery further away from the well bore than can be monitored by wireline logs. The differential pressure across plug **A** during the initial brine injection stabilised around Δp = 70 kPa which decreased to Δp = 20 kPa during the AS injection. No subsequent increase was observed, contrary to the poor injectivity found in the field [5]. Similar pressures were observed for the EOR process in plug **B**.

The influence of capillary end effects on the bulk oil saturation determined in such short plugs can be negated by considering recovery in a central region of the plug [6]. In Figure 3, we divide the plug profiles into three regions of equal volume (inlet, middle, outlet) and consider the oil recovery from each region separately. This detailed analysis is possible with the inclusion of a spatial dimension in the NMR experiments. The middle region is indicative of recovery occurring in an infinite volume (i.e., no capillary end effects) where the final oil saturation at the end of the flood is S_{or} = 17 s.u. This oil saturation is the same in the outlet region once the AS has removed the capillary end effect, but prior to AS injection the oil saturation in the outlet region is approximately 5 s.u. higher than in the middle and inlet regions. On AS injection, the formation of an oil bank is observed, and its progress is visible through the inlet, middle, and outlet regions. By the end of the flood, the oil saturation at the inlet is reduced (compared to the middle/outlet) to S_{or} = 12 s.u.

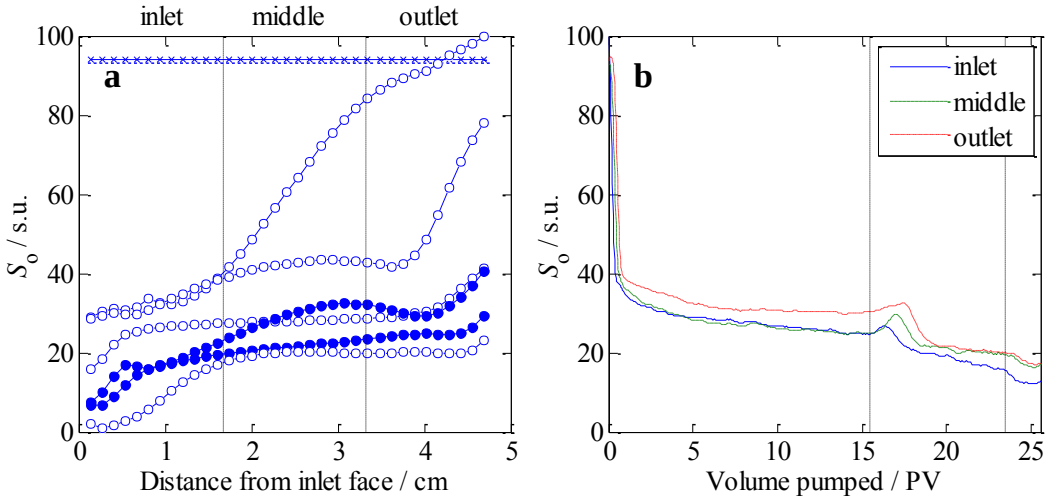

Figure 3. Localised oil saturations determined for plug **A**. A selection of profiles acquired during the flood is shown in (a) (fluid flow left to right). All profiles are normalized relative to the initial oil saturation to remove consistent image artefacts. The flood progressed from top to bottom (PV=0, 1, 3, 10, 17, 22, 25) with profiles acquired at initial saturation (×), during water flood (○), and during AS flood (●). In the first of the AS flood profiles, the oil bank (increased S_o) is visible. The profiles are divided into three regions (inlet, middle, outlet) and the variation in oil saturation for each of these regions is shown in (b). AS injection occurred between the vertical dashed lines. $S_{or}^{(w)}$ at the outlet is higher than for the rest of the plug due to the capillary end effect. The middle and the outlet regions equilibrate after AS injection. During the initial brine flood, the inlet and middle are well matched, although the oil saturation at the inlet decreases during and after the AS injection, attributed to the formation of a microemulsion. The middle region is considered equivalent to a bulk saturation measurement in a long core-plug where end effects are unimportant.

At the onset of AS injection (15.4 PV cumulative injected volume), see Figures 2 and 3, the remaining oil saturation is seen to increase. This increase is attributed to the presence of the protonated co-solvent. The T_2 distributions obtained from the bulk CPMG experiments, Figure 4 (left), reveal an increase in the intensity of the short T_2 component on AS injection. This short relaxation time is used to distinguish the oil and co-solvent, allowing a corrected bulk remaining oil saturation to be calculated, see Figure 4 (right). The co-solvent present in the rock is persistent at a saturation of 3 s.u. during the AS injection, consistent with the concentration of DGBE in the bulk AS formulation. We assume, therefore, that the co-solvent does not become trapped in the rock or associate with slow moving oil. The same level of analysis was not possible with the T_2 dimension of the y-T_2 maps due to the low SNR of these data and long echo times.

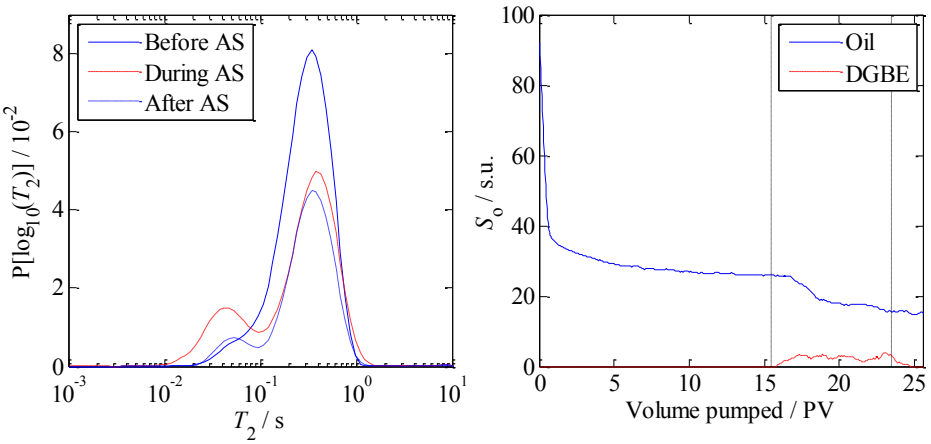

Figure 4. Bulk specimen T_2 relaxation time distributions (left) obtained at various stages through the flood of plug **A**. The oil exhibited a predominantly monomodal distribution between 0.1 s < T_2 < 1 s, with a small tail extending down to T_2 = 0.01 s. On injection of the AS, a separate T_2 component became distinguishable between 0.01 s < T_2 < 0.1 s. The increase in intensity of this component was attributed to the co-solvent (DGBE). After AS injection, the intensity of this component was reduced; the persistent signal was attributed to oil trapped in the smallest pores. The additional intensity in the short component was used to differentiate the oil and co-solvent present in the rock (right); the S_o scale is relative for the DGBE. The S_o is bulk ROS corrected for DGBE, and no longer shows the elevated saturation at the onset of AS injection observed in Figure 3. The co-solvent saturation does not exceed 3 s.u., equivalent to the 3 wt% present in the bulk AS. This saturation implies the co-solvent is distributed evenly through the rock and does not accumulate during continued injection of AS.

The progress of the co-solvent through the rock is not intrinsically related to the progress of the active surfactant component in the AS. The recovery of the surfactant was determined by analysis of the effluent. The variation in surfactant concentration observed for plug **A** is shown in Figure 5. There is a slight delay (equivalent to 1.5 – 2 PV injected fluid) between the start of the AS injection and significant surfactant recovery, suggesting the surfactant is held up in the rock, possibly due to partitioning into the oil or association with a micro-emulsion. The total surfactant recovery was equal to 78 % of the injected volume, although continued brine flooding may have recovered additional surfactant. In plug **B** where 2.4 PV of AS were injected, only 55 % of the surfactant was recovered, suggesting an initial portion of the surfactant is adsorbed or partitions into the oil.

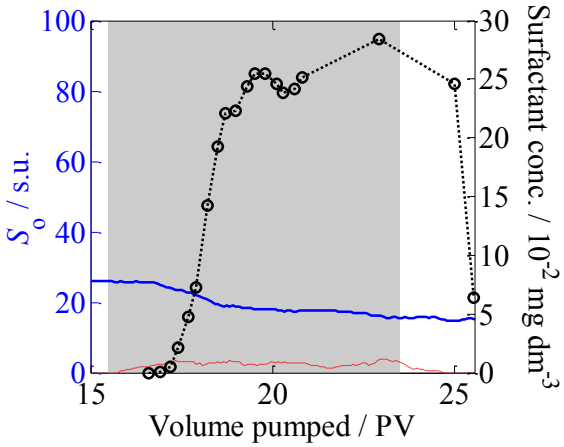

Figure 5. Concentration of surfactant (Petrostep S-8A) in the aqueous fluid-phase of the effluent recovered from flood of plug **A** (black circles and dotted line). There is a delay of approximately 2 PV between AS injection (grey rectangle) and significant surfactant recovery, suggesting some hold-up in the rock. The co-solvent (red dashed line) present in the rock is repeated from Figure 4; the remaining oil saturation is also repeated (blue line) for comparison. The initial surfactant recovery coincides with enhanced oil recovery (reduction in S_o), suggesting the surfactant is transported with the oil. The total recovered surfactant volume was equal to 78 % of the injected volume. Surfactant may be lost by partitioning into the oil, adsorption on pore surfaces, or associated with a micro-emulsion.

Discussion

This study shows the importance of a spatial resolution of the flood geometry in addition to the measurement of oil saturation. Fluid-phase-specific NMR provides the saturation; MRI methods provide the spatial resolution. The combination of saturation with spatial resolution is also important at larger length scales.

At the next scale, in the single-well *in situ* EOR evaluation [2,3,5], an electric image of the flooded zone and oil bank accompanies saturation logs made by NMR and an array dielectric dispersion tool. Based on the electric image logs, it is possible to determine when the tool sensitive volumes are completely in the flooded zone. Interpreting for ROS without knowledge of the flood geometry puts such interpretations in doubt. In [5], the NMR log after AS injection was in the event abandoned because the antenna would not have resolved the small volume flood. At the largest length scale possible in single-well tests, a log-inject-log pilot was performed with the same AS through perforated casing [4]. Two saturation measurements were: chemical tracers in the Single Well Chemical Tracer (SWCT) and time-lapsed pulse neutron capture (PNC) logs. Relevant spatially resolved data are however very limited for SWCT and PNC.

In Table 3 we compare the methodologies at various length scales, and the resulting ROS measurements. We see that the SWCT [4], single-well pilot [5], and laboratory study all gave similar ROS after the chemical flood, a very satisfactory agreement.

The main discrepancy lies in the higher ROS values from PNC logs recorded across the perforated interval [4] (Table 3). These showed minimal change between water and chemical floods. One explanation is suboptimum hydraulic isolation, shown by the cement bond log. The injected brine and AS may have swept a deeper zone in the reservoir, connected by a channel in the annulus. This does not invalidate the SWCT measurement however; if the brine, ester solution and alkaline surfactant all sweep the same volume of formation, the change in ROS will still be valid. The fluid routes are guesswork. When the partitioning ester and the injected chemicals have different viscosities (e.g. with chemical floods that include thickening polymers), the assumption that the fluids traverse the same formation is weakened. The interpretation of shallow

cased hole saturation logs such as PNC, recorded across perforated casing, also relies on an unverified assumption of flood geometry. The schematic, Figure 6, illustrates.

Table 3. Comparison of ROS measured at length-scales probed in core floods and two types of single-well pilots. Shown are saturations after waterflood $S_o^{(w)}$ at nominal 1 PV flood volume, and also $S_{or}^{(w)}(\infty)$ at end of waterflood. Data from Figs. 4 (right) and 5. Residual oil after chemical flood $S_{or}^{(c)}$ is not available from NMR only because flood volumes were too low in [5]. Except for a determination of initial saturation, measurement effluent volumes are unreliable in this case because of evaporation of volatiles.

Mode	Context	Imaging method	Length-scales probed	Saturation magnitude	$S_o^{(w)}$ (x PV) / s.u.	$S_{or}^{(w)}(\infty)$ / s.u.	$S_{or}^{(c)}$ / s.u.
core flood	Laboratory	MRI	~ cm	NMR effluent vols.	36 (1 PV)	25	17
Single-well pilot (log-drill-inject-log)	open hole	Electric Image	~ dm	NMR Dielectric dispersion	32 (3–4 PV) n/a		n/a 18
Single-well chemical tracer	cased hole	n/a	~ m ~ dm	SWCT PNC	35 (~ 1 PV) 58		19 57

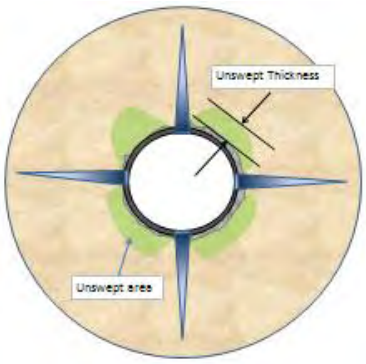

Figure 6. Residual oil unswept next to casing between perforations, by-passed by flow through perforations. The PNC depth of investigation is shallower than the perforation penetration depth. Hence PNC logging after EOR surfactant injection may not measure the true (low) ROS. Note the perforations are staggered along the borehole, not in one plane. Staggering makes the phenomenon even more likely than sketched. The presence of induced micro-fractures at the tip of the perforations is likely to increase the volume of near-wellbore unswept oil.

There could be both under swept oil and over swept oil; under swept in the shadow zones between the perforations, and over swept at the perforations where the capillary numbers are high. Bypass creates non-uniformity in chemical EOR where the remaining oil moves only when contacted by the EOR agent. Independent measurement of flood geometry details is impossible; the ideal environment for these cased hole measurements, is from a hydraulically isolated observation well that does not participate in the dynamics of the surfactant flood.

Laboratory-scale studies also demonstrate the importance of having two independent saturation measurements to corroborate quantification, using entirely different physical principles. In core floods like those reported, these are NMR and effluent volumetrics. Evaporation of volatiles was difficult to control in the present case and therefore not

reported, though correctable with improved collection apparatus. For the single-well *in situ* EOR evaluation [3] they are NMR and dielectric dispersion. Cased-hole tools that provide PNC measurements can also measure the ratio of carbon to oxygen from gamma ray energy resulting from inelastic scattering of fast neutrons. However, ROS from SWCT relies on just one measurement: the shift between the partitioning tracers.

Conclusions

Quantitative EOR evaluation has been demonstrated on the laboratory-scale using low-field NMR, with spatial resolution by image profiling (MRI). The spatial dimension is important at all EOR piloting length-scales, but is especially important when studying short core-plugs for which bulk volumetrics may be dominated by capillary or geometry end effects, and yield wholly incorrect ROS values (though remaining valuable for corroborating the accuracy of saturation measurements). The ROS after chemical flood, $S_{or}^{(c)}$, observed in the middle of a short core-plug, was consistent with that observed during single well pilots in the actual reservoir, using dielectric dispersion measurements in the single-well *in situ* EOR evaluation [5] (dm length scale), and also in the Single Well Chemical Tracer [4] (producing interval length scale). These observations add confidence to the ROS measurement, through corroboration over a wide range of length-scales. The discrepant PNC cased-hole logs are explicable by uncertain fluid flow paths.

Redundancy in saturation measurement physics similarly adds confidence when results are quantitatively similar. In the single-well *in situ* EOR evaluation [2,3,5] the measurements of choice are NMR and dielectric dispersion. In this reservoir [5], NMR was not run after injection (because of limited flood volume) but ordinarily will be. Laboratory core floods with NMR monitoring at low magnetic fields then provide a valuable calibration of the NMR logs, in addition to the direct assessment of ROS.

We conclude that corroboration with multiple length scales, spatial resolution, and correspondence with preferred logging measurement physics, all contribute to the value of NMR-monitored core-floods as a complement to field pilot studies.

References

1. W.M. Stoll, H. al Shureqi, J. Finol, S.A.A. Al-Harthy, S. Oyemade, A. de Kruijf, J. van Wunnik, F. Arkesteijn, R. Bouwmeester, M.J. Faber, "Alkaline / surfactant / polymer flood; from the laboratory to the field," *SPE Reservoir Evaluation & Engineering*, (2011) December, 702-712.
2. S. Arora, D. Horstmann, P. Cherukupalli, J. Edwards, R. Ramamoorthy, T. McDonald, D. Bradley, C. Ayan, J. Zaggas, K. Cig, "Single-well in-situ measurement of residual oil saturation after an EOR chemical flood," *SPE EOR conference at Oil and Gas West Asia, Muscat, Oman, 11-13 April*, (2010) Paper SPE 129069.
3. R. Ramamoorthy, M. Kristensen, J. Edwards, C. Ayan, K. Cig, "Introducing the MicroPilot: moving rock flooding experiments downhole", *SPWLA India 3rd Logging Symposium*, 25-26 November (2011).

4. H. Soek, M. Jaboob, M. Singh, A. Jabri, M. Stoll, R. Faber, K. Al Harthy, R. Al Mjeni, J. van Wunnik, "Plans for chemical Enhanced Oil Recovery in a North Oman carbonate field", *SPE Middle East Oil and Gas Show, Manama, Bahrain, 25-28 September*, (2011) Paper SPE 139537.
5. J. Edwards, R. Ramamoorthy, E. Harrigan, M. Singh, H. Soek, J. van Wunnik, M. Al Yarabi, R. Al Mjeni, "Single-well in-situ measure of oil saturation remaining in carbonate after an EOR chemical flood", *SPE Middle East Oil and Gas Show, Manama, Bahrain, 25-28 September*, (2011) Paper SPE 141091.
6. J. Mitchell, J. Staniland, R. Chassange, E.J. Fordham, "Quantitative in-situ enhanced oil recovery monitoring using magnetic resonance" *Transp. Porous Med.* (2012) Accepted for publication.
7. D.N. Saraf, I. Fatt, "Three-phase relative permeability measurement using a nuclear magnetic resonance technique for estimating fluid saturation," *SPE J.* (1967) September, 235-242.
8. A. Brautaset, G. Ersland, A. Graue, J. Stevens, J. Howard, "Using MRI to study in-situ oil recovery during CO_2 injection in carbonates," *SCA* 2008-41.
9. D.P. Green, J.R. Dick, M. McAloon, P.F. de J. Cano-Barrita, J. Burger, B.J. Balcom, "Oil/water imbibition and drainage capillary pressure determined by MRI on a wide sampling of rocks," *SCA* 2008-01.
10. J. Mitchell, T.C. Chandrasekera, M.L. Johns, L.F. Gladden, E.J. Fordham, "Nuclear magnetic resonance relaxation and diffusion in the presence of internal gradients: the effect of magnetic field strength," *Phys. Rev. E* (2010) **81**, 026101.
11. J. Mitchell, P. Blümler, P.J. McDonald, "Spatially resolved nuclear magnetic resonance studies of planar samples," *Prog. Nucl. Magn. Reson. Spect.* (2006) **48**, 161-181.
12. H. Carr, E. Purcell, "Effects of diffusion on free precession in NMR experiments," *Phys. Rev.* (1954) **94**, 630-638.
13. S. Meiboom, D. Gill, "Modified spin-echo method for measuring nuclear relaxation times," *Rev. Sci. Instrum.* (1958) **29**, 668-691.
14. S. Davies, K.J. Packer, "Pore-size distributions from nuclear magnetic resonance spin-lattice relaxation measurements of fluid-saturated porous solids. II. Applications to reservoir core samples," *J. Appl. Phys.* (1990) **67**, 3171-3176.
15. J.P. Butler, J.A. Reeds, S.V. Dawson, "Estimating solutions of 1st kind integral-equations with nonnegative constraints and optimal smooting," *SIAM J. Num. Anal.* (1981) **18**, 381-397.
16. G. Wahba, "Practical approximate solutions to linear operator equations when data are noisy," *SIAM J. Num. Anal.* (1977) **14**, 651-667.
17. P.T. Callaghan, *Prinicples of nuclear magnetic resonance microscopy*, Claredon, Oxford, (1991).
18. P. Majors, P. Li, E. Peters, "NMR imaging of immiscible displacements in porous media," *SPE Form. Eval.* (1997) **September**, 164-169.
19. American Public Health Association, American Water Works Association, Water Pollution Control Federation, *Standard Methods for the examination of water and wastewater*, American Public Health Association, 18th ed. (1992).